Experimental determination of the stability diagram of a lamellar eutectic growth front

Marie Ginibre, Silvère Akamatsu, and Gabriel Faivre
Groupe de Physique des Solides, CNRS URA 17, Universités Denis-Diderot et Pierre-et-Marie-Curie, Tour 23, 2 place Jussieu, 75251 Paris Cedex 05, France

(Received 18 November 1996; revised manuscript received 14 February 1997)

We present an experimental study of the growth patterns of directionally solidified thin samples of the lamellar eutectic alloy CBr_4-C_2Cl_6 as a function of the pattern wavelength λ, the solidification velocity V, and the alloy concentration C, within the so-called planar coupled zone of the parameter space. Capillary-anisotropy effects and three-dimensional (3D) effects are minimized by an appropriate choice of the eutectic grain size, the eutectic grain orientation, and the sample thickness. We first verify the old proposition made by Jackson and Hunt [Trans. AIME **236**, 1129 (1996)] that the basic patterns (i.e., the stationary, spatially periodic, reflection-symmetric, 2D patterns) of our system are stable over a finite range of λ at given V and C, the lower bound of which is determined by a local, lamella-termination instability. We show that the upper bound of the basic state stability range is marked by a primary Hopf bifurcation toward an oscillatory state. The nature of the oscillatory state, and the threshold value for the bifurcation, depend on C. Other, secondary bifurcations occur at higher λ. In total, we identify six different types of low-symmetry extended growth patterns: the already-known steady symmetry-broken, or ''tilted'' state [K. Kassner and C. Misbah, Phys. Rev. A **44**, 6533 (1991); G. Faivre and J. Mergy, *ibid.*, **45**, 7320 (1992)], and five new types of oscillatory and/or tilted states. We determine the stability domains of the various states in the plane $(C,\lambda V^{1/2})$, and characterize the various primary and secondary bifurcations of our system. Our experimental results are in good quantitative agreement with the stability diagram numerically calculated by Karma and Sarkissian [Metall. Mater. Trans. **27A**, 635 (1996)] in the frame of a 2D model without capillary anisotropy. [S1063-651X(97)10107-6]

PACS number(s): 64.70.Dv, 81.10.Fq, 03.40.−t

I. INTRODUCTION

When solidified from the melt, a binary eutectic alloy yields a two-phase solid. The average proportion of the two phases is fixed by mass conservation, but their spatial arrangement, called the solidification microstructure of the alloy, is of a dynamical origin: it is the trace left behind in the solid by the dynamical patterns that the growth front assumed in the course of the solidification. When both crystal phases grow from the melt in a fully diffusion-controlled way, when the alloy concentration C is sufficiently close to the center of the eutectic plateau, and when the solidification is performed directionally at constant velocity V under a sufficiently strong thermal gradient G, the solidification microstructure usually consists of a regular alternation of planar lamellae of the two crystal phases running parallel to the growth direction—the alloy is then called a lamellar eutectic [1]—indicating that the growth front assumed a stationary periodic growth pattern during solidification. An example observed during the directional solidification of a thin sample of the transparent eutectic alloy CBr_4-C_2Cl_6, is shown in Fig. 1. The phase diagram of this alloy is reproduced in Fig. 2. The method of observation is directional solidification of thin samples. A 12-μm-thick layer of CBr_4-C_2Cl_6 enclosed between two glass plates is placed in an externally imposed unidirectional temperature gradient, and pulled at an imposed velocity toward the cold side of the gradient. The front, which is in a steady state, and is therefore immobile in the laboratory reference frame, is observed from above with an optical microscope. The two phases composing the lamellae are the α and β phases appearing at the edges of the eutectic plateau. The growth pattern shown in Fig. 1 is stationary, periodic in the direction normal to the lamella plane, two-dimensional (2D), i.e., translation invariant in the direction normal to this plane, and reflection symmetric about the planes bisecting the lamellae. (Hereafter, the terms periodic and period, when used without further specification, always refer to spatial periodicity. It is current practice to call the width of the ''unit cell'' of the basic state, i.e., of a pair of lamellae, interlamellar spacing, or, simply, spacing.) We shall call the patterns of this type ''basic patterns'' or ''basic states'' of directionally solidified lamellar eutectics, in contradistinction with the patterns of lower symmetry to be studied later on in this article.

The experimental investigation of lamellar eutectic growth presented in this paper primarily aims at answering the question of the stability of the basic (type of) pattern as a function of its interlamellar spacing λ at given values of V,

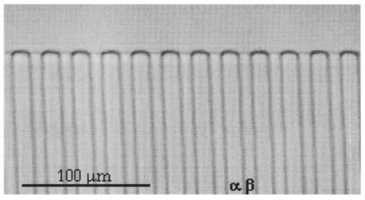

FIG. 1. Directionally solidified thin sample of the eutectic alloy CBr_4-C_2Cl_6 in a basic state. Reduced concentration: $\eta \approx 0.4$. Pulling velocity: $V = 0.5\ \mu m\ s^{-1}$. Interlamellar spacing: $\lambda = 23.5\ \mu m$. Anisotropy-driven tilt angle: $\phi \approx 1.5°$ to the left. (See text for explanations.) In this, and all the following photographs, the growth direction is upward. The α lamellae can be distinguished from the β ones thanks to the darker contrast of their interface with the liquid.

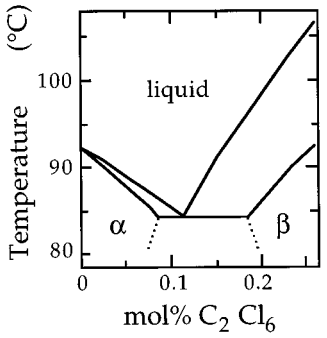

FIG. 2. Phase diagram of the alloy CBr_4-C_2Cl_6 [18]. The crystal structures of the two terminal solid solutions α and β are face-centered-cubic and body-centered-cubic, respectively.

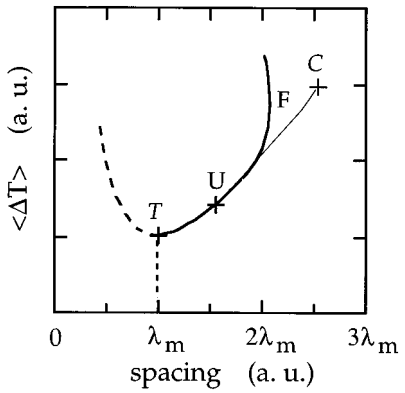

FIG. 3. Average undercooling of the growth front vs interlamellar spacing in the basic state (sketch). Jackson and Hunt's view was that the basic state was stable from T (lamella termination) to C (''catastrophic change'') [6]. It is now established that the basic state grows unstable at some spacing U (upper stability bound), and that the basic-state branch ends at a higher spacing F (fold).

G, and C. This is an old question, which has long been considered as a matter for metallurgy (many metallic alloys of industrial interest are lamellar eutectics), and now is mostly the concern of the physics of nonlinear dynamical systems [2]. We consider that the present paper, in conjunction with the numerical work recently published by Karma and Sarkissian [3], answers this question, at least for 2D systems. Therefore, we should begin by briefly recalling the main previous stages of the resolution of the problem.

The fundamental study of lamellar eutectic growth began about half a century ago [4]. At the beginning of the 1960s, extensive experimental investigations on directionally solidified metallic eutectic systems had led to a number of questions, in particular, the following ones: (i) What is the part played by the anisotropy of the crystal phases in lamellar eutectic growth? It had indeed been proved that this part is not a major one, but the exact nature of the ''anisotropy effects'' remained totally unclear (progress has recently been made on this problem, as will be seen later on in this paper). (ii) What is the origin of the fact that, at given C, directionally solidified lamellar eutectics appear to select a relatively well-defined value of their spacing, proportional to $V^{-1/2}$ and independent of G. (iii) What is the origin of the observed deviations from the perfect regularity of the basic pattern, which seemed to be in disagreement with the preceding observation [5]? The fundamental problem underlying the last two questions is that of the stability of the basic pattern as a function of λ. This was first stressed by Jackson and Hunt in 1966, in a paper which has remained the principal reference as regards the fundamental aspects of lamellar eutectic growth [6]. The experimental method of directional solidification of thin samples of transparent alloys, and the so-called minimal model of lamellar eutectic growth [7], which are still currently used, were introduced in that paper. It is therefore needful to briefly, but accurately, recall what was then put forward concerning the stability problem of the basic pattern.

In the frame of the minimal model, and with the help of some additional simplifying approximations, which were later shown not to be crucial, Jackson and Hunt demonstrated that the equations of growth admit basic (i.e., stationary, periodic, 2D, symmetric) solutions for a large range of values of λ at given V. They calculated the average undercooling of the front as a function of λ. This function goes through a minimum at a value λ_m of the spacing, called the minimum-undercooling spacing. The approximate value of λ_m found by Jackson and Hunt, thereafter denoted λ_{JH}, is proportional to $V^{-1/2}$ and independent of G. Jackson and Hunt did not attempt to perform the stability analysis of the basic solutions, but gave a plausible, heuristic, discussion of this problem. They argued that (i) the lower stability bound of the basic state was probably an instability leading to the elimination of a lamella (lamella termination) and should occur at λ_m; and that (ii) the upper stability bound should correspond to a ''catastrophic change'' of the shape of the lamella tips leading to the creation of a new pair of lamellae, and should occur at $A\lambda_m$, where A is a C-dependent numerical coefficient larger than 2. Figure 3 summarizes these ideas. Noting that the order of magnitude, and the V dependence of λ_m, roughly coincide with the experimentally observed ones, Jackson and Hunt concluded that directionally solidified lamellar eutectics generally grow near the minimum-undercooling condition. Jackson and Hunt moreover considered this conclusion as supporting the old minimum-undercooling principle according to which, when several possible solidification regimes exist for a given system, the system tends to select the regime with the lowest undercooling. We shall return to this more controversial idea in the conclusion of this paper.

Jackson and Hunt's arguments were perfectly consistent, but their assumption concerning the upper stability bound of the basic state has now been disproved. It is now certain that the basic state grows unstable (and even ceases to exist; see Fig. 3), at a spacing smaller than that at which the ''catastrophic change'' was predicted by these authors to occur, and that the corresponding mode of instability does not lead to the creation of new lamellae. So, above the upper stability bound of the basic state and below the threshold of any lamella-creating instability, there exists a finite interval of λ, inside which the system can permanently remain in a variety of low-symmetry patterns. The first hints of this were found in 1981 by Datye and Langer [8], who discovered theoretically the period-doubling oscillatory (2λO) mode of instability of the basic state, and in 1987 by Karma, who confirmed this finding numerically, and moreover discovered

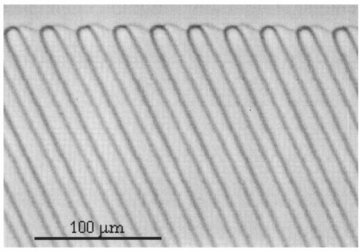

FIG. 4. Tilted pattern. $\eta=0.45$. $V=0.8\ \mu\mathrm{m\,s^{-1}}$. $\lambda=29\ \mu\mathrm{m}$ ($\Lambda\approx1.6$). $\phi=24.5°$. Since there is no appreciable mass diffusion in the solid, the lamellae left behind in the solid can be viewed as a materialization of the space-time diagram of the growth front.

the tilt (T) mode of instability [9] (see also [10]). These findings opened new prospects to the fundamental study of lamellar eutectic growth. A few years ago, following Jackson and Hunt and other authors [11,12], our group undertook an experimental investigation of the solidification dynamics of thin samples of the alloy CBr_4-C_2Cl_6 [13–19]. At the same time, several other groups (mostly, Caroli and Caroli [20–22], Kassner and Misbah [23–28], Karma and Sarkissian [3], and co-workers) pursued the theoretical study of lamellar eutectic growth analytically and numerically. Among other results, it was established numerically by Kassner and Misbah in 1991 [25], and experimentally by Faivre and Mergy in 1992 [16], that, at the particular alloy concentration corresponding to the center of the eutectic plateau, CBr_4-C_2Cl_6 presents a homogeneous tilt bifurcation at $\lambda\approx1.9\lambda_m$. At spacings larger than this value, the basic state is unstable, while a tilted periodic state is stable (Fig. 4). The tilt angle ϕ of the lamellae in this state, defined by $\tan\phi=V_d/V$, where V_d is the lateral traveling velocity of the pattern, is in the range $25°-35°$. It was also shown experimentally that, at the same concentration, the system undergoes a period-doubling oscillation in a narrow range of spacing around $1.2\lambda_m$.

We have pursued our experimental investigation of directionally solidified thin samples of CBr_4-C_2Cl_6 more systematically, researching the possible periodic states of this system as a function of λ, V, and C. In other words, we determined experimentally the 2D stability diagram of CBr_4-C_2Cl_6 within the ''planar coupled zone'' of the parameter space [29]. (In the context of the eutectic growth, the term ''planar'' refers to the aspect of the front on a scale much larger than λ). At the same time, Karma and Sarikissian calculated this diagram numerically, with the help of a dynamical code enabling them to study not only the existence, but also the stability of the states [3]. The values of the material parameters of CBr_4-C_2Cl_6 recently (re)measured by Mergy *et al.* [18] were used in the calculations. This paper is mostly devoted to the presentation of the experimentally determined stability diagram of our system, and to the comparison with Karma and Sarkissian's numerically calculated diagram. To avoid possible misunderstandings, it must be immediately specified that these diagrams do not take into account all the existing permanent states of our system, but only the 2D homogeneous ones. We call homogeneous pattern, a pattern extending over the whole width of the sample, or, at least, over a width of, typically, 100 λ, and deviating from perfect periodicity only through the frozen-in spatial modulations of λ explained in Sec. III of this article. Within the planar coupled zone of the parameter space, lamellar eutectics also admit nonhomogeneous and 3D types of growth patterns. Some of these are mentioned below, but they are not studied in any detail.

This paper is organized as follows. The reduced variables that we use for the presentation of the results, and the ranges of these variables scanned in this study are defined in Sec. II. The experimental methods, and the main experimental sources of error are explained in Sec. III. The presentation of the experimental stability diagram, and the comparison with Karma and Sarkissian's numerical results are carried out in Sec. IV. Section V is devoted to the dynamics of the system near the bifurcation thresholds. Some general conclusions are given in Sec. VI. Let us point out that Sec. III not only contains technical indications, but also original pieces of information on the process of formation of the eutectic grains and the frozen-in spatial λ modulations, and the description of an original method of elaboration of single-grained samples. Reminders of some previously established, important properties of lamellar eutectic growth (inefficiency of phase diffusion, rearrangement of the spatial distribution of the spacing through the emission of tilt domains, the part played by capillary-anisotropy and 3D effects), can also be found in this section. We also wish to stress that we consider the good quantitative agreement between the experimental and the numerical stability diagrams established in Sec. IV as the main result of this study. In comparison, the information on the bifurcation transients presented in Sec. V is still fragmentary. The most striking features of these bifurcations, namely, the localized dynamical objects (tilt domains, solitary tilt waves, oscillation pulses, phase defects) associated with them, remain to be studied in detail, with the exception of tilt domains [17].

II. SIMILARITY LAW AND REDUCED VARIABLES

An important, specific property of lamellar eutectic growth is the similarity law stating that, at given C, any value of the spacing defined by some well-defined property (e.g., minimum of the undercooling, bifurcation threshold) is proportional to $V^{-1/2}$ and independent of G. This law is far from being strictly valid, as will be seen shortly. However, it is a valuable simplifying approximation in the region of the parameter space that we consider here. We shall adopt it below, unless otherwise specified. In other words, we shall most of the time admit that the type of pattern adopted by our system depends only on two variables, $\lambda V^{1/2}$ and C. It is common practice to reduce these variables in a manner which facilitates comparisons between different lamellar eutectic alloys. For this purpose, one defines the reduced concentration as

$$\eta=\frac{C-C_\alpha}{C_\beta-C_\alpha}, \tag{1}$$

where C_α and C_β are the concentrations at the edges of the eutectic plateau, and the reduced spacing as

$$\Lambda=\frac{\lambda}{\lambda_{\mathrm{JH}}}\propto\lambda V^{1/2}. \tag{2}$$

where λ_{JH} is the Jackson-Hunt minimum-undercooling spacing, which has already been defined. Instead of η, one may use the reduced deviation from eutectic concentration $\Delta=\eta-\eta_E$, where η_E is the value of η at the eutectic concentration C_E (in our case, $\eta_E\approx 0.29$; see Fig. 2), or the reduced deviation from the center of the eutectic plateau $\Delta'=\eta-0.5$. Note that η is equal to the molar fraction of β phase of a solid at equilibrium with the liquid at the eutectic temperature T_E. Because the variation of the undercooling of the front as a function of λ over the basic-state stability range is very small (typically 10^{-3} K), it is not possible to determine experimentally λ_m (or λ_{JH}) directly. The scaling factor $\lambda_{JH}V^{1/2}$ has thus to be calculated from the value of η and the following physical constants of the system: the diffusion coefficient D of the solute in the liquid, the surface tensions of the three types of interface, and the quantities pertaining to the phase diagram [6]. These constants were recently measured in the alloy CBr_4-C_2Cl_6, with the help of, in particular, a study of the shape of the front in the basic state as a function of λ [18]. In the range $0.1<\eta<0.6$, the experimentally determined value of $\lambda_{JH}V^{1/2}$ can be fitted by

$$\lambda_{JH}V^{1/2}\approx(13.84-4.9\Delta'+57\Delta'^2-285\Delta'^3+847\Delta'^4)\ \ \mu\mathrm{m}^3\ \mathrm{s}^{-1}. \tag{3}$$

The uncertainty is about 10%, independently of η.

Concerning the conditions of validity of the similarity law $\lambda\propto V^{-1/2}$, the following result was recently established by Kassner and Misbah [23]. Consider the reduced shape of the front, i.e., the function $\lambda^{-1}\zeta(\lambda^{-1}x)$, where x is the space variable in the lateral direction, and ζ the position of the front along the growth direction. In a steady periodic state, this shape depends on the three dimensionless parameters Λ, $P=\lambda V/D$, and $\chi=DG/\Delta TV$, where $\Delta T=m_\alpha(C_\alpha-C_E)$, and $m_\alpha(<0)$ is the slope of the α liquidus (for simplicity, a symmetrical phase diagram is assumed). Kassner and Misbah showed that, in the limit $P\to 0$, the reduced shape only depends on Λ and χ. Moreover, when χ is small, the dependence on χ is negligible. So, there are indeed quantities (e.g., λ_m), which, under some conditions, virtually depend on the sole variable Λ (at given concentration). These conditions are, roughly speaking, $P<0.1$, $\chi<1$, and $\Lambda<2$. They are fulfilled in our experiments, and it was accordingly experimentally verified that the similarity law satisfactorily applies to the front shapes in the basic state of our system [18]. On the other hand, it is now experimentally established that there are also quantities that do not follow the law $\lambda\propto V^{-1/2}$. This is the case of the spacing dynamically selected by tilt domains (the definition of this quantity is recalled in Sec. III B), which roughly follows a V^{-1} law [17], and of the threshold spacing for the 2λO bifurcation, as shown in Sec. V C of this paper. In the following, we present our results in the form of maps drawn in the plane (Λ,η). Projected onto this plane, deviations from the law $\lambda\propto V^{-1/2}$ cause an apparent scatter between data measured at different velocities. However, in our case, this scatter turns out to be sufficiently small not to blur the limits of the stability domains.

All the experiments reported below were performed at $G=80\pm 5$ K cm^{-1}. G being fixed, a concentration-dependent upper bound is imposed to the explored values of V by the eutectic-dendrite and the planar-colonies transitions (see Ref. [29]). In our case, this bound ranges from about 2.5 to 10 μm s^{-1}. All the observations presented below were obtained in the range $0.3<V<3$ μm s^{-1} [with the exception of Fig. 20(b), for which $V=6.3$ μm s^{-1}]. On the other hand, we restricted ourselves to the concentration and spacing ranges corresponding to $0.1<\eta<0.6$ and $\Lambda<3$.

III. EXPERIMENTAL METHODS

A. Experimental procedure

The primary aim of this study was to determine the nature of the stable homogeneous states of our system as a function of C, λ, and V. The experimental procedure that we applied for this purpose takes advantage of the following properties of our system: (i) the above-mentioned similarity law $\lambda\propto V^{-1/2}$, (ii) the particular process of formation of the initial state of the system, (iii) the inhibition of the mechanisms of creation of new lamellae in thin samples, and (iv) the ineffectiveness of phase diffusion. These properties are by no means common to all the 1D modulated fronts, but are specific of lamellar eutectic growth. We shall return to them shortly. How they come into play in the following experimental procedure is however obvious. We first pull the sample at a velocity V_0 for a sufficiently long time for the system to reach an initial steady state, which is a basic state at a spacing close to λ_{JH} and therefore depending on V_0. Then we suddenly increase V by a sufficiently small quantity for not triggering creations of lamellae or tilt domains (an upward V jump). This leaves the average and the local values of λ practically unchanged. The reduced spacing Λ is thus multiplied by a factor equal to the square root of the amplitude of the V jump, defined as the ratio of the growth velocities after and before the V jump. We wait for a possible instability to grow, and, when this happens, for the system to restabilize in a different type of pattern. Further upward or downward V jumps can then be applied. Each experimental run is thus supposed to give us a series of points representing the permanent states of the system for different values of $\lambda V^{1/2}$ at a given C. We performed many such experiments with various values of the concentration and spacing, until the interesting zone of the parameter space was satisfactorily scanned. In practice, numerous difficulties complicate this idealized picture.

B. Uncertainties of technical origin

The technical details about the solidification setup and the preparation of the samples can be found elsewhere [14–18,30,31]. We must, however, recall the following facts. Our samples are made of two parallel glass plates separated by plastic spacers, delimiting an empty space about 8 mm wide, 70 mm long, and 12 μm thick (36-μm-thick samples were also occasionally used). This space, filled with the molten alloy, fixes the external dimensions of the system. The glass plates are not perfectly planar. The sample thickness undergoes variations of, typically, 3 μm over distances of the order of 1 cm. These variations have no detectable effect on

the dynamics of the system. The optical images of the growth front are continuously recorded with the help of a camera and a videotape recorder, and then processed and analyzed with a Power Macintosh computer using the public domain NIH Image program (developed at the U.S. National Institutes of Health and available from Internet by anonymous FTP from zippy.nimh.nih.gov or on floppy disk from the National Technical Information Service, Springfield, Virginia, Part No. PB95-500195GEI).

The pulling speed is communicated to the sample by a dc motor *via* a micrometric screw. The instantaneous value of V is measured by following the motion of inert features of the sample. At constant rotation speed of the motor, the average value of V is constant to within less than 1%, but the instantaneous value undergoes a periodic variation of about $\pm 4\%$ of the average value. This is due to some residual misalignment in the pulling system, as shown by the fact that the time period of the V modulation corresponds to a turn of the pulling screw (1 mm). This time period (typically, 10^3 s) is noticeably larger than the time periods of the oscillations in the oscillatory states (typically, 30 s). In some cases, we detected a variation of the amplitude of the oscillations over times comparable with the time period of the V modulation. This was not a resonance, but a quasistatic adaptation of the system to the instantaneous value of V. In all the cases considered below, the modulation of V could be safely ignored.

The interlamellar spacing is measured on the images as the distance between two successive homologous junction points at the interface. The reading uncertainty on each position is about 0.5 μm, corresponding to a relative uncertainty of a few percent on each individual value of λ. Since the measured values of λ generally correspond to averages over several contiguous periods, the error on the values of λ given below is generally smaller than 1%, and negligible in comparison with the other sources of errors. In presenting the results in terms of $\Lambda=\lambda/\lambda_{\rm JH}$, we add the relative error on $\lambda_{\rm JH}$ to the reading uncertainties on λ. Since this error on $\lambda_{\rm JH}$ is practically independent of η over the explored range of η, it simply corresponds to an error on the scaling factor of the ordinates in the diagrams (η,Λ).

The alloy concentration is redetermined *in situ* by measuring the ratio of the width of the β lamellae to λ in the basic state. The theoretical value of this ratio is practically equal to η [6,20]. The absolute reading uncertainty ranges from about 0.02 to 0.05, depending on the value of λ and the homogeneity of the pattern. In relative value, the error on η is thus by far the largest of the reading errors made on the control parameters. Measuring η *in situ* allows us to trace the residual concentration gradients that may exist in the liquid prior to the onset of the solidification. These gradients turn out to be always larger near the ends than in the central part of the samples. Therefore, only a portion of the samples about 20 mm long, located at equal distances from its ends, was used in the experiments. In this region, the concentration gradients, expressed in terms of η, were at most of the order of 10^{-4} per spacing. This is very small in comparison with the gradients generated by the growth itself. In most cases, the residual concentration gradients are thus unlikely to perturb the local growth dynamics significantly. We also followed the concentration transients subsequent to the V jumps [32]. These transients die out rapidly, and therefore pose no serious experimental problem. However, over distances of the order of the sample width, or the solidified length, the variations of η are not negligible. Care was taken to refer the results to the local, instantaneous values of η.

Finally, in some cases, evaporation and contamination [31] cause the molten alloy to deteriorate slowly with time. For this reason, as a general rule, a different sample, and thus a different eutectic grain, were used for each solidification run. On the other hand, neither λ nor η can be chosen entirely at will, as can easily be understood from the preceding. In other words, we do not fully control the way in which the plane (Λ,η) is scanned. We therefore had to use a large number of samples (about 100). In spite of this, our exploration of the plane (Λ,η) presents some, fortunately not important, deficiencies.

C. Origin of the frozen-in λ modulation and the eutectic grains

Our ultimate purpose being to compare the experimental observations with numerical calculations performed in the frame of the minimal model, we also had to meet with difficulties arising from the fact that some physical properties of the experimental system are not taken into account in this model. These are the following:

(i) The frozen-in λ modulation. By this, we designate the nonuniform spatial distribution of the spacing, which is generated during the initial stages of the solidification run, and which, because of the phase-diffusion ineffectiveness, persists without noticeable modification, at least as long as the tilt mode of instability is not activated.

(ii) The capillary-anisotropy effects. In the process of solidification, the anisotropy of the solid phases comes into play via the orientation dependence of the surface tensions (capillary anisotropy), which itself intervenes via the eutectic-grain microstructure of the samples. We recall that a eutectic grain is a region of the sample, of size generally much larger than λ, within which all the lamellae of the same crystallographic type (i.e., α or β) have the same orientation of their crystal lattice [33]. Our nontreated samples, like those of any lamellar eutectic, are divided into a certain number of eutectic grains, separated from each other by sharp boundaries called eutectic grain boundaries.

(iii) The residual 3D effects. In these we include all the dynamical phenomena that involve deformations of the growth front in the direction perpendicular to the glass plates (transverse direction).

Prior to explaining how we tackled these effects, we must briefly describe the initial stages of the solidification, during which the eutectic grains and, simultaneously, the frozen-in λ-modulation, are formed. Such a description has never been given before, to our best knowledge. Consider, say, a hypoeutectic sample ($C<C_E$). Before the start of a solidification run, the sample is allowed to sit at rest for about 1 h in the thermal gradient. At the end of this homogenization annealing, the solid in contact with the liquid is entirely in the excess phase (α, in the chosen example), but is not a single crystal. The grain size inherited from the previous history of the sample is about 100 μm. At rest, the front sits at the temperature $T_f=T_E+m_\alpha(C-C_E)>T_E$. When the pulling is started at the desired velocity V_0, the front first ''recoils'' in

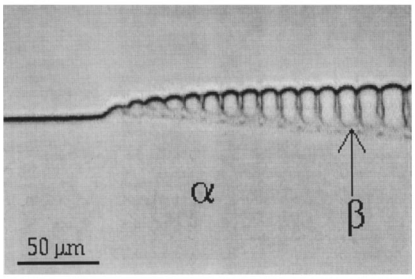

FIG. 5. Oscillatory invasion process during the early stages of a solidification run. $\eta=0.12$. $V=0.8\ \mu\mathrm{m\ s^{-1}}$ ($\lambda_{JH}\approx 25\ \mu\mathrm{m}$). The incipient lamellar pattern appearing in this figure is unstable against lamella termination.

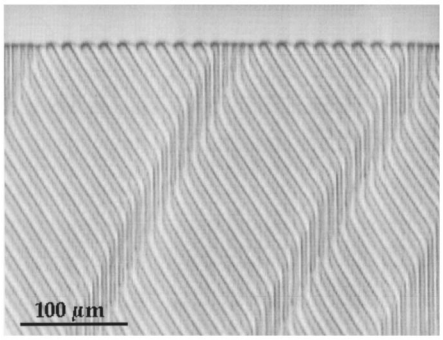

FIG. 6. Tilt domains alternating with basic-state domains. $\eta=0.5$. $V=0.84\ \mu\mathrm{m\ s^{-1}}$.

the laboratory reference frame (T_f decreases) under the effect of the accumulation of solute in the liquid [34]. When T_f reaches T_E, it becomes thermodynamically possible that the β phase coexists with the α phase at the solid-liquid front. In the conditions of our experiments, β appears in the form of a small single crystal located at one of the cusps created by the grain boundaries emerging at the α-liquid interface. The mechanism through which this occurs involves the migration of the β phase from some β grain situated far behind the growth front up to this front along one of the liquid channels associated with the grain boundaries [14]. The front is then rapidly invaded by the β phase. It can be seen in Fig. 5 that the invasion is accompanied by a 3D oscillation, which gives rise to the periodic emission of branches from the underlying α crystals. The branches have the same crystal orientation as the mother crystal, so that there exists a one-to-one correspondence between the final eutectic grains and the initial α grains (the β lamellae have the same orientation in all the grains, while the α lamellae have the orientation of the underlying α grains). Moreover, the probability of one of these grains having its α and β lamellae in, or close to, an epitaxial orientation relationship is quite small. So, according to the terminology proposed in Ref. [15] (see also Ref. [35]), all the grains generally are of the ''floating'' type, i.e., they have a weak, nonsingular orientation dependence of the surface tension of the α-β interface (the α-liquid and β-liquid interfaces, which are rough on the molecular scale, always fulfill this condition).

Eutectic grains apart, the immediate results of the oscillatory invasion process is a periodic lamellar structure of the basic-state type. The spacing of this pattern is much smaller than the lamella-termination threshold at the velocity V_0, which is close to λ_{JH}. The process therefore continues by a series of loosely correlated lamella termination events. This, and the absence of phase diffusion, explain that the system finally reaches a steady state, in which λ is everywhere close to λ_{JH}, and spatially modulated in an irregular way. Typically, the characteristics wavelength of this spatial modulation is $10\lambda_{JH}$, and its amplitude $0.1\lambda_{JH}$. So the frozen-in λ gradients are, at most, of a few 10^{-2}. It turns out experimentally that, while the nonlinear effects due to such gradients are probably unimportant, the variations of λ from place to place along the front are sufficient to complicate the interpretation of the observations. This is fortunately often compensated for by the local character of the dynamics, i.e., the slaving of the local state of the system to the local value of λ [16]. Examples are given below.

We mentioned above that the spatial λ distribution of our samples can be strongly modified if, and, practically, only if, the tilt mode of the instability is triggered. The most spectacular way in which such rearrangements take place is by the emission of tilt domains. A detailed experimental description of this phenomenon can be found elsewhere [13,17]. For our present purpose, it suffices to recall the following. A tilt domain is an inclusion of a stable tilted state in a stable basic state. The values of the spacing inside and outside the domain are appreciably different from each other (see Fig. 6). Tilt domains travel along the front in the direction opposite to that of their internal states. The emission of a tilt domain, i.e., the formation of a tilt domain in a region of the front, and its subsequent traveling away from this region, results in a net decrease of the spacing in the region from which the tilt domain is emitted. The sweeping of the front by tilt domains leaves the system in a basic state at a well-defined, unique value of the spacing λ^* at given V. This is the so-called dynamical selection of the wavelength [36]. A train of tilt domains is shown in Fig. 6. The tilt domains shown in this figure are of different width, but each of them travels at constant width, indicating that the dynamical wavelength selection has already been accomplished by the previous passage of other tilt domains. Dynamical wavelength selection only takes place under some conditions (existence of a stability range of the tilted state, stability of the selected basic state, existence of sources from which tilt domains are emitted). When these rather restrictive conditions are fulfilled, dynamical wavelength selection can be used to get rid of the initial λ modulations.

D. Size and anisotropy of the eutectic grains

Capillary anisotropy breaks the mirror symmetry of the isotropic system considered by the ''minimal'' theoretical model. Consequently, the reflection symmetry of the basic state itself is broken. In other words, in the basic state of real lamellar eutectics, there exists a nonzero ''anisotropy-driven'' tilt angle ϕ of the pattern [15] (see Fig. 1). This angle is of course grain dependent. In a given (floating) grain, it increases as λ increases. Each grain can be characterized from the point of view of its capillary anisotropy by the value ϕ_m of ϕ at $\lambda=\lambda_m$. In CBr_4-C_2Cl_6, ϕ_m ranges from 0° to about 5° (in absolute value). Capillary anisotropy

can also modify the values of the bifurcation thresholds, and even the nature of the bifurcations [16,26]. These effects, which are obviously uniform within a given grain, and different in different grains, are quantitatively poorly known as yet. We are therefore reduced to treating them as a source of dispersion arising between data originating from different grains. In order to minimize this dispersion, we selected eutectic grains showing a low value of ϕ_m (less than $2°$).

A further, indirect effect of capillary anisotropy is that eutectic grain boundaries are sources of steep local λ gradients, and of various other defects, in particular, tilt domains [15]. It is thus of primary importance to reduce the number of eutectic grains as much as possible. For this purpose, we utilized the so-called method of successive invasions (in fact, we combined this new method with the use of funnel-shaped spacers [30]). We stated above that the primary lamellar structure is generated by the 3D oscillation accompanying the invasion of the front by the default phase (β, in the example of Fig. 5). In fact, at sufficiently low pulling velocity, the 3D oscillation does not occur. Then, at the end of the invasion, the solid among the front is a single crystal of the β phase. It can be easily understood that the newly formed β front must in turn be invaded by the α phase. [Incidentally, successive invasions are the basic ingredient of the oscillatory growth regimes (''giant oscillations'') occurring at Λ larger than about 3 [14]. These regimes will be studied in a forthcoming paper.] By increasing V at the moment when this second invasion begins, one can impose that it is accompanied by 3D oscillations, i.e., by the projection of β lamellae from the underlying β *single* crystal. Ideally, the result of this two-step treatment is a single eutectic grain extending over the whole width of the sample. In general, we did not obtain this ideal result, but reduced the number of grains to, typically, two. The size of the largest grain was then about 5 mm, which is sufficient for our purpose. The final result can be checked by stopping the solidification momentarily, and waiting for a single-phased front to reform. The residual grain boundaries (if any) are then revealed by the cusps that they form at the solid-liquid interface (see Fig. 7 of Ref. [15]). It should, however, be noted that subgrain boundaries (grain boundaries of disorientation less than about a degree) are not detected by this method.

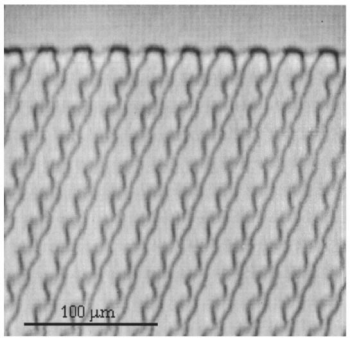

FIG. 7. Tilted, period-preserving oscillatory ($T-1\lambda O$) pattern. $\eta=0.35$. $V=1.55$ μm s^{-1}. $\lambda=26$ μm ($\Lambda\approx2.35$). $\phi\approx23°$. Time period: $t\approx35$ s.

E. Three-dimensional effects

The primary reason for using very thin samples is to block the convection flows in the liquid that necessarily exist in bulk samples. Direct observation shows that there is no convection flows in samples less than about 50 μm thick [32]. On the other hand, in sufficiently thin samples, the lamellae in the basic state are always perpendicular to the glass plates, that is, parallel to the transverse direction, while, in thick samples, the lamellae are generally at an angle (called twist angle) with respect to this direction. It is found experimentally that the last condition (lamellae normal to the glass plates) is more stringent than the preceding one (no convection), and is only satisfactorily fulfilled in samples less than some 20 μm thick.

The unlocking of the lamella plane with respect to the normal to the glass plates as the sample thickness is increased can be explained as follows. We observed that, in thick samples, the twist angle of the lamella is roughly uniform inside a given eutectic grain, but different in different grains, indicating that it is fixed by capillary anisotropy. On the other hand, two effects may contribute to forcing the lamella plane to remain perpendicular to the glass plates, namely, the confinement of the system by the glass plates, and the wetting forces at the glass plates (confinement and wetting effects). The strength of the capillary effects is independent of the sample thickness, while that of the confine-

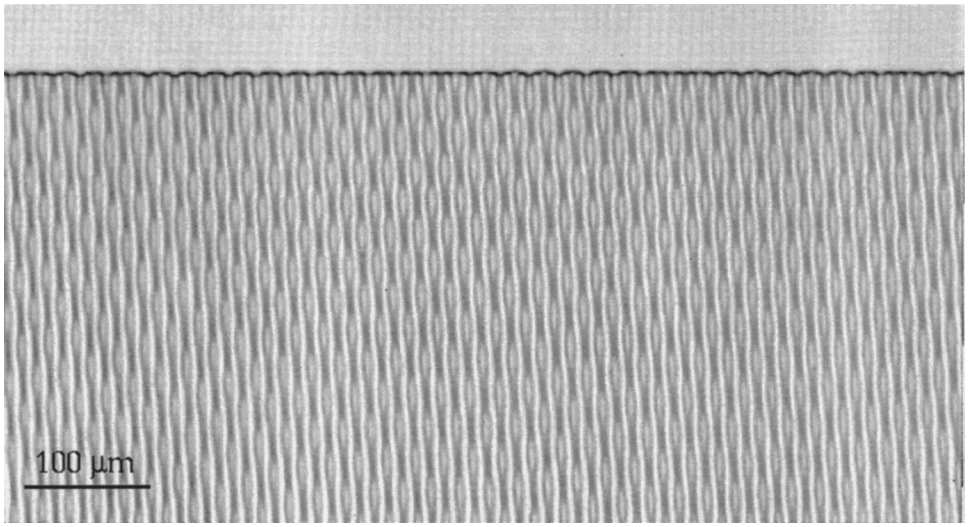

FIG. 8. Homogeneous period-doubling oscillatory ($2\lambda O$) pattern. $\eta=0.48$. $V=1.52$ μm s^{-1}. $\lambda=12$ μm ($\Lambda\approx1.1$). $t\approx35$ s.

ment and wetting effects increases as the sample thickness decreases, which accounts for the transition.

More generally, the confinement and the wetting effects tend to inhibit all the 3D modes of instability of the basic state. Observations allowed us to roughly quantify this last effect. In our system, the 3D modes of instabilities are practically blocked when the ratio t/λ is smaller than about 1.5. In 12-μm-thick samples, and for the velocity range used here, most of the λ thresholds of the 2D bifurcations fulfill the condition $t/\lambda<1.5$. Therefore, no 3D instability generally occurs during our experiments. It must, however, be stressed that some 3D instabilities do occur in our samples under some specific conditions, for instance, the instability responsible for the creation of new lamellae. This point of a great practical importance deserves a detailed comment.

The only type of lamella-creation mechanism occurring systematically in 12-μm-thick samples of CBr_4-C_2Cl_6 is a local mechanism called lamella branching [19]. In brief, this consists of the invasion of a wide α lamella showing a deep trough at its tip (which occurs for Λ larger than about 2.5) by a branch projected by one of the adjacent β lamellae. Experimentally, it is clear that the process is a 3D one. A new lamella could be created without a 3D deformation of the growth front only through the nucleation of a new crystal in the liquid, but this cannot occur in the conditions specific of lamellar eutectic growth (the critical undercooling of heterogeneous nucleation of crystals from the melt is always much larger than the undercooling at the bottom of any realistic trough along the front). The process is not the result of a linear instability of some homogeneous state, but of a ''dynamical nucleation.'' That is, lamella branching occurs as the result of generally rare, local events, which themselves preferentially take place at some specific sites of the sample (e.g., eutectic grain boundaries). An example of lamella branching triggered by large-amplitude 2λ oscillations can be seen in Fig. 23 below. Other examples can be found elsewhere [13]. In our large-grained, 12-μm-thick samples, and at sufficiently small pulling velocities, lamella branching can be totally avoided. It is then possible to study the growth dynamics of lamellar eutectics up to arbitrary large values of Λ, but this will not be done here.

IV. STABILITY DIAGRAM

A. 2D periodic patterns

We have experimentally identified three 2D modes of instability in directionally solidified thin samples of CBr_4-C_2Cl_6. These are the tilt (T), the period-doubling oscillatory (2λO) and the period-preserving oscillatory (1λO) modes. We have moreover observed the three modes corresponding to the simultaneous activation of two of the pure modes. These ''mixed'' modes will be denoted T-2λO, T-1λO, and 1λ-2λO, respectively. We have also encountered oscillatory tilt modes of wavelength longer than 2, denoted T-$x\lambda$O [37].

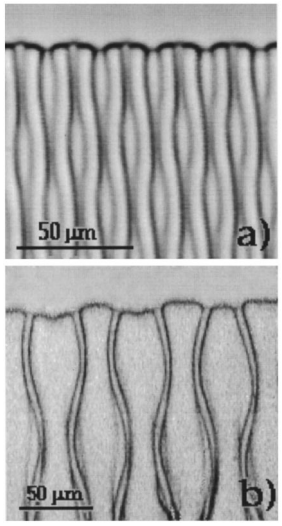

FIG. 10. Large-scale views of 2λO patterns. (a) Hypereutectic sample (same run as in Fig. 8). (b) Hypoeutectic sample [$\eta=0.2$. $V=1\ \mu\mathrm{m\,s^{-1}}$. $\lambda=29\ \mu$m. ($\Lambda\approx1.7$). $t\approx110$ s.]

The first question that we considered, once a given type of mode of instability was identified, is whether or not it can give rise to a permanent, homogeneous pattern. This question was previously answered in the positive as concerns the T pattern (see Fig. 4) [16]. This state is easily obtained over the whole width of the sample, and then remains indefinitely homogeneous. In other words, the frozen-in λ modulation and the slight nonuniformity of the concentration of our samples do not lead to a destabilization of this type of state. The same statement applies to the T-1λO pattern (Fig. 7). Conversely, the 2λO state was long only obtained in the form of transient patches (the same observation was made before in other lamellar eutectic systems [12,38]). Through successive improvements of the homogeneity of our samples (see Sec. III), we finally succeeded in obtaining instances of quasipermanent, homogeneous 2λO patterns. An example is shown in Fig. 8. In this particular case, the 2λO pattern extended over some 600 basic periods. The homogeneity was only broken by a slight, spatial variability of the time period, detectable in Fig. 8, and by the occurrence of a few local

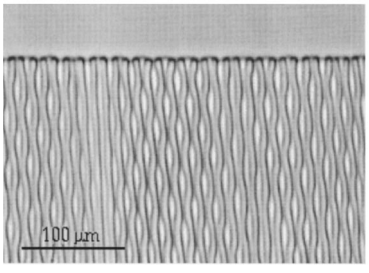

FIG. 9. Phase defects in a 2λO pattern. Same run as in Fig. 8.

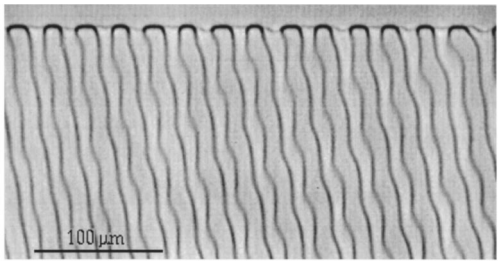

FIG. 11. Tilted, period-doubling oscillatory ($T-2\lambda$O) pattern. $\eta=0.44$. $V=0.7\ \mu\mathrm{m\,s^{-1}}$. $\lambda=26.6\ \mu$m ($\Lambda\approx1.6$). $\phi\approx8°$. $t=67$ s.

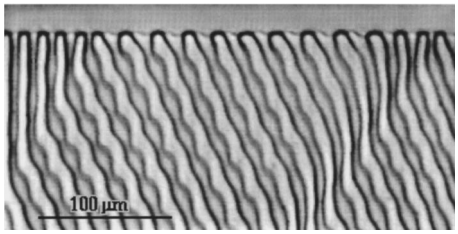

FIG. 12. Oscillations of wavelength longer than 2λ in a tilt domain (T-xλO domain). $\eta=0.5$. $V=1.7$ μm s^{-1}. $\lambda=23$ μm ($\Lambda\approx2.1$). $\phi=23°$. $t=23$ s.

defects through which the phase of the oscillation changes by π (Fig. 9). There is thus no doubt that the 2λO pattern is a stable periodic state of our system at the appropriate values of λ, η, and V. It is to be noted that, in the 2λ oscillations, one type of lamella follows a wavy trajectory, while the other remains reflection symmetric. Figure 10 shows large-scale views of two 2λO states observed one in a hypereutectic, the other in a hypoeutectic sample. It can be seen that the symmetry-broken lamellae are those of the default phase (α in the hypereutectic range, β in the hypoeutectic range). This statement applies even when the phase fraction of this phase is larger than 0.5, which is the case for the β phase when η is between η_E and 0.5.

An example of $T-2\lambda$O pattern is shown in Fig. 11. The tilt angle in this type of state is typically 10°. Like the 2λO state, a homogeneous T-2λO state filling the whole sample is difficult to obtain. It is, however, easy to obtain this state in wide, homogeneous domains. We also observed domains of oscillatory states of the T-xλO type, where x is larger than 2. An example, in which $x\approx6.3$, is given in Fig. 12. We encountered practically all the types of patterns ranging from the T-2λO to the T-1λO type (the latter is the limit of the T-xλO type at $x\to\infty$). The domains in which the T-xλO patterns were observed were all of a relatively small width (typically, 10 λ). It is therefore not certain that states of this type are really stable, and if they would be found to decay slowly with time if observed in larger domains.

Figure 13 shows a region of the front in a 1λO state. A view of a larger field would show that the oscillation amplitude is not spatially uniform. This is due to the slaving of the oscillation amplitude to the underlying frozen-in modulation of the spacing, as shown below. The 1λO state would thus be obtained in a perfectly homogeneous form if the amplitude of the frozen-in λ modulations was reduced. Figure 14 shows a region of the front in the 1λ-2λO mixed state. The quasiperiodic or chaotic (a precise characterization could not be done) behavior visible in this figure is perhaps induced by the nonuniformity of the spacing.

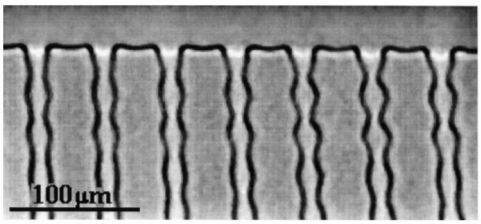

FIG. 13. Period-preserving oscillatory (1λO) pattern. $\eta=0.28$. $V=0.5$ μm s^{-1}. $\lambda=50$ μm ($\Lambda\approx2.5$). $t=70$ s.

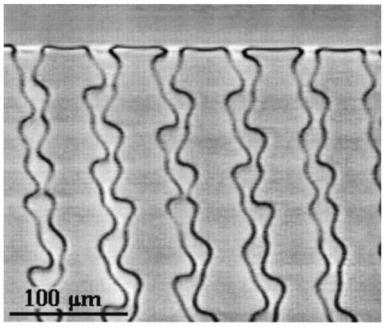

FIG. 14. 1λO-2λO pattern (see text). $\eta=0.28$. $V=0.46$ μm s^{-1}, $\lambda=60$ μm ($\Lambda\approx2.7$). The slight tilt of the pattern ($\phi\approx6°$) is perhaps spontaneous, i.e., not induced by capillary anisotropy. The pattern would then in fact be of a T-1λ-2λO type.

The 1λO mode of oscillation may rightly be called an ''optical mode'' of oscillation of the basic state. It should, however, not be confused with another mode of oscillation, which was also called ''optical mode'' in a previous publication [39], but which, to avoid confusion, we shall call here the ''oscillatory pinching'' of the minority lamella. This other mode is shown in Fig. 15. It indeed essentially consists of an oscillation of the width of the β lamellae, but, contrary to the 1λO mode, (i) it is observed at relatively low values of η and Λ; (ii) it is a local mode, in the sense that each β lamella oscillates practically independently from its neighbors; and (iii) observations not reproduced here show that it has an important 3D component. The range of η in which the oscillatory pinching takes place suggest that it is in some way connected with the lamella-rod transition, which would take place in bulk samples in the same range of η [6]. This will, however, have to be confirmed by further studies. For now, the important point is that the oscillatory pinching does not seem to be a collective, 2D mode of oscillation of our system, in agreement with the fact that it has not been found numerically.

In directionally solidified thin samples of monotectic alloys at very small fractions of the low-temperature liquid phase, Grugel, Lograsso, and Hellawell [40] observed an oscillatory mode reminiscent of our oscillatory pinching. Conversely, the ''optical mode'' found by Gill and Kurz in the laser solidification of the Al-Al_4Cu eutectic at nearly equal fractions of the two phases [41] seems similar to the 1λO mode of our system.

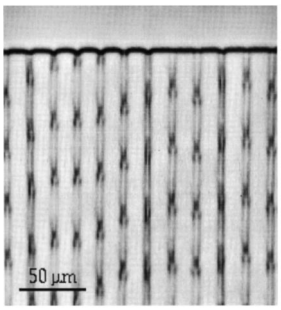

FIG. 15. Oscillatory pinching of the β lamellae. $\eta=0.15$. $V=2.34$ μm s^{-1}. $\lambda\approx18$ μm ($\Lambda\approx1.3$). $t=18$ s.

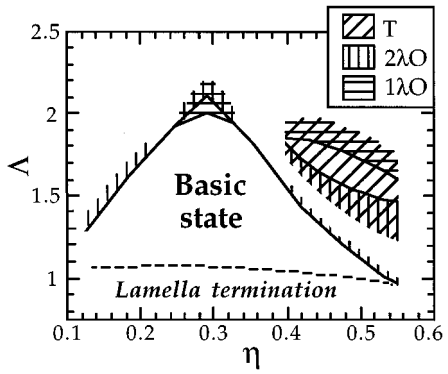

FIG. 16. Stability diagram of directionally solidified CBr_4-C_2Cl_6 numerically calculated by Karma and Sarkissian [3]. η: reduced concentration. Λ: reduced spacing. η and Λ are dimensionless variables.

B. Numerically calculated stability diagram [3]

Before we turn to a comparison of the experimentally determined stability domains of the periodic patterns with those numerically calculated by Karma and Sarkissian, we should briefly sum up the results recently published by these authors [3]. Karma and Sarkissian's calculations were performed at fixed values of V and G ($V=11.95\ \mu\mathrm{m\,s^{-1}}$, $G=187.9\ \mathrm{K\,cm^{-1}}$) for a number of values of λ and Δ. The size of the system was 2λ, and periodic boundary conditions were applied. For each point (Δ,λ) considered, the authors observed that, after a transient, the system reaches some type of permanent state. They determined the stability boundaries of the various states by studying the evolution of the decay rate of small perturbations as a function of λ at fixed Δ.

The stability diagram found by Karma and Sarkissian is shown in Fig. 16. In order to facilitate the comparison with our results, we have transformed the original (λ,Δ) data kindly communicated to us by the authors into (Λ,η) data, as explained in Sec. II. We have replaced the discrete set of calculated points by hatched regions (for the stability domains) and continuous lines (for the stability boundaries) by means of interpolations. The errors thus introduced are totally unimportant for our present purpose. The three pure modes of instability are represented by specific types of hatching, and the mixed modes by the superposition of two types of hatching. Some of the hatched areas are not delimited by continuous lines on all sides because the corresponding stability boundaries have not been numerically determined. Two cases call for a particular comment. The boundary that one expects to find between the 2λO and T-2λO domains on the hypereutectic side of the diagram could not be determined because lamella termination was found to occur when approaching this boundary from downward. Some insight into the dynamics of the system in this region could nevertheless be gained by calculating the stability diagram of a 1λ-wide system, i.e., a system in which the 2λO mode was blocked. The upper stability limit of the basic state was then raised to a higher value, corresponding to the threshold of the supercritical, pure tilt bifurcation (T bifurcation) previously calculated by Kassner and Misbah [25]. The second particular comment concerns the lower stability boundary of the basic state. Karma and Sarkissian did not systematically look for this boundary, but made a preliminary calculation on a 10-λ-wide symmetrical system (see below) showing that the lamella-termination instability predicted by Jackson and Hunt to take place at λ_m actually occurs at Λ smaller than about 0.9. The lamella termination threshold, which generally (but not always; see Sec. VI) coincides with the lower stability boundary of the basic state, is thus certain to lie somewhat below the broken line draw in Fig. 16, which represents the minimum-undercooling reduced spacing $\Lambda_m=\lambda_m/\lambda_{\mathrm{JH}}$.

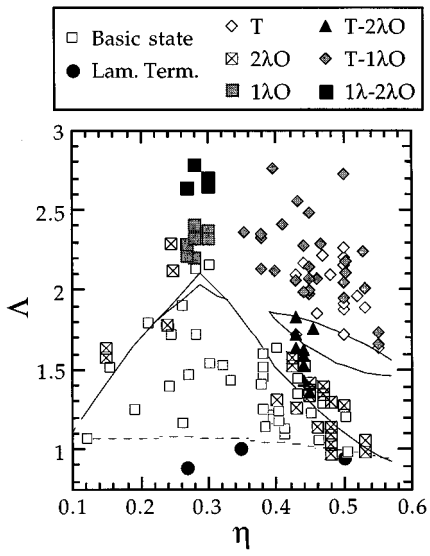

FIG. 17. Stability diagram of directionally solidified CBr_4-C_2Cl_6. Points: experimentally observed periodic patterns. Lam. Term.: lamellar termination. Curves: numerically calculated diagram (see Fig. 16).

Karma and Sarkissian also calculated the stability diagram of a fictitious, fully symmetrical, eutectic alloy. The features that this symmetrical system shares with CBr_4-C_2Cl_6 can be considered as common to all the lamellar eutectics. These are as follows: (i) The width of the basic-state stability range is at a maximum in a small zone around the eutectic point. (ii) In this zone, the primary bifurcation is to the 1λ O state, and is rapidly followed by a secondary bifurcation to the mixed 1λ-2λO state. (iii) On either side of this central zone, the primary bifurcation is to the 2λO state, and the threshold of this bifurcation decreases rapidly as $|\Delta|$ increases. (iv) Sufficiently far away from the eutectic point, the stability domain of the basic state ceases to exist. On the other hand, no stability domain of the tilted states appear in the symmetrical diagram, indicating that the existence of such domains on the hypereutectic side of the CBr_4-C_2Cl_6 diagram stems from the relatively strong asymmetry of the phase diagram of this system. This property is probably shared by many strongly asymmetric binary eutectics.

Finally, Karma and Sarkissian calculated the bifurcation diagrams (oscillation amplitude vs spacing diagrams) of the primary 1λO bifurcation at $\Delta=0$, and of the 2λO bifurcation at $\Delta=0.1$ in the case of the symmetrical model alloy. Both bifurcations are slightly subcritical. The width of the metastability domain is $\delta\Lambda\approx0.08$ for the 1λO bifurcation and $\delta\Lambda\approx0.03$ for the 2λO bifurcation. In the latter case,

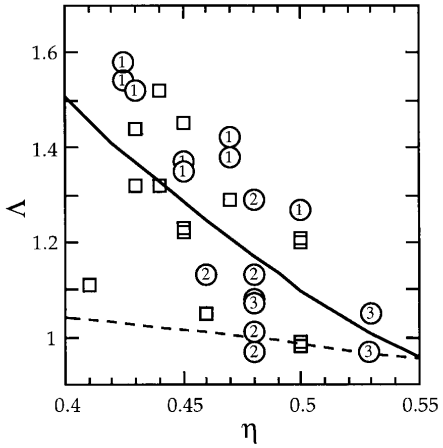

FIG. 18. Enlarged particular of Fig. 17. Open squares: basic state. Open circles: 2λO states. Labels 1, 2, and 3 correspond to $V \approx 0.5$, 1.5, and 2.2 μm s^{-1}, respectively. The 2λO points obtained at other values of V are not represented.

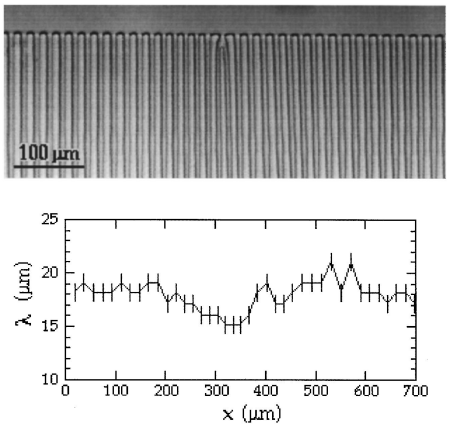

FIG. 19. Photograph: isolated lamella-termination event. $\eta = 0.5$. $V = 0.4$ μm s^{-1} ($\lambda_{JH} \approx 22.3$ μm). Graph: plot of the spacing as a function of position prior to the event. The lamella termination occurred at $x \approx 330$ μm (the field in the graph is larger than in the photograph).

lamella termination occurs at $\delta\Lambda \approx 0.06$ above the upper bifurcation threshold.

C. Experimental stability diagram

The (η, Λ) points corresponding to all the periodic states that we observed, excluding the T-xλO ones, are displayed in Fig. 17, superimposed on the numerical diagram. Typically, we did not obtain the oscillatory states, which are fragile to long-wavelength perturbations, in a fully permanent, extended form. The points appearing in Fig. 17 correspond to patterns extending over more (usually, much more) than ten interlamellar spacings, and lasting longer than ten oscillation time periods. An enlarged view of the most entangled part of the diagram is shown in Fig. 18 (the special symbols used in this figure will be explained in a moment). Data corresponding to lamella-termination events are also reported in Fig. 17 (filled circles). They give the highest values of λ at which isolated lamella-termination events were observed in a given solidification run. The corresponding events were isolated, and occurred after a long transient (Fig. 19).

Qualitatively, the agreement between experiments and numerical calculations is obviously good. The same types of state are found in the same regions of the parameter space. The general features listed at the end of Sec. IV B are all confirmed experimentally. From the quantitative standpoint, however, two types of discrepancies between experiments and calculations appear. The first one is an overall dilatation of about 12% of the experimental Λ scale with respect to the numerical one. This is obviously explainable by the uncertainty with which λ_{JH}, the scaling factor of the ordinates, is known. It would suffice, for instance, to multiply the value of D taken in the calculations by a factor of about 1.2 to make the experimental and theoretical Λ scales coincide satisfactorily. The second type of discrepancy is the large extension of, and the large overlaps between, the experimental stability domains. Such overlaps, if real, would indicate that the corresponding bifurcations are subcritical, with wide domains of metastability, which was not found theoretically. In fact, except perhaps in the case of the $T \rightarrow T$-1λO bifurcation, the overlaps appearing in Fig. 17 are all explainable by the experimental uncertainties discussed in Sec. III, and by the fact that some oscillatory regimes do not follow the law $\lambda \propto V^{-1/2}$. The detailed study of the bifurcation dynamics presented in Sec. V leaves no doubt about this point. More details can be given in the case of the primary 2λO bifurcation. It will be shown below that the threshold of this bifurcation approximately follows a $\lambda \propto V^{-0.7}$ law. The corresponding values of Λ should therefore be corrected by a factor $(V/\overline{V})^{0.2}$, where $\overline{V}$ is some (arbitrary) reference value of V. It can be seen in Fig. 18 that applying such a correction actually allows one to reduce the apparent overlap between the basic-state and the 2λO-state stability domains in the plane (η, Λ). However, the overlap remaining after this correction is applied (attributable to the reading errors on η and the dispersion resulting from the grain-dependence of the capillary parameters) still is much larger than the width of the metastability domain estimated in Sec. V A.

In conclusion, it can be stated that a complete, quantitative agreement exists between the experimental and the numerical stability diagrams, within experimental uncertainties. It must, however, be kept in mind that these uncertainties are relatively large. They forbid us, for instance, to draw any conclusion about the subcritical or supercritical nature of the bifurcations from Fig. 17.

V. PRIMARY AND SECONDARY BIFURCATIONS

A. 2λO primary bifurcation

We have studied experimentally the response of our system to small-amplitude V jumps in the region of the 2λO threshold in hypereutectic and hypoeutectic samples. This study necessitated the development of special methods of image analysis because of the very narrow range of spacing in which 2λ oscillations show up. The methods, and the results obtained, will be described in detail elsewhere [42]. Here we shall only give an outline of our conclusions. Two types of response are observed. The most usual one is as follows (Fig. 20). The 2λ oscillations appear locally, at, or near, the maximums of the frozen-in λ modulation, spread out in a way which was previously described by Zimmer-

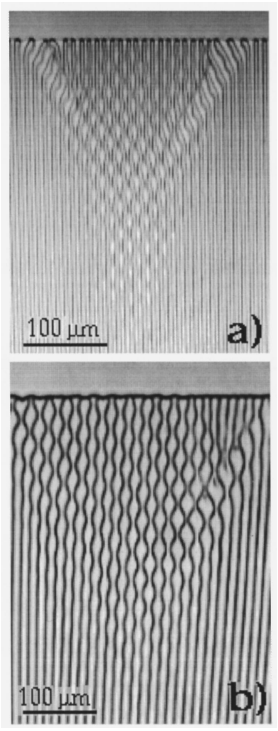

FIG. 20. Generation of period-doubling oscillations subsequent to a small-amplitude increase of V. (a) Hypereutectic sample. $\eta=0.5$. $V=2.25\ \mu\mathrm{m\ s^{-1}}$. $\lambda=10.5\ \mu\mathrm{m}$ ($\Lambda\approx1.1$). Two tilt domains are propagating to either sides of the figure. (b) Hypoeutectic sample. $\eta=0.15$. $V=6.3\ \mu\mathrm{m\ s^{-1}}$. $\lambda=11.3\ \mu\mathrm{m}$ ($\Lambda\approx1.4$). A solitary tilt wave is propagating to the rightmost side of the figure.

mann, Karma, and Carrard [38], and then trigger the emission of tilt domains or solitary tilt waves, i.e., localized, traveling objects of a definite width. Examples are shown in Fig. 20 (we turn to the distinction between domains and solitary waves at the end of Sec. V B). The emission of tilt domains or waves results in a decrease of the spacing in the region from which they are emitted, hence in a decrease of the oscillation amplitude. It can thus be seen that the process is a complicated one, which involves the interplay between the 2λO and T modes via the rearrangement of the spatial distribution of λ. We shall not linger on it here.

The second type of response is shown in Fig. 21. The 2λ oscillations appear in the form of broad, intermittent patches, which are not obviously connected to underlying bumps of the λ modulation, and which do not end in tilt

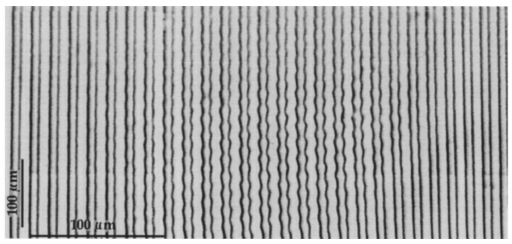

FIG. 21. Transient patch of period-doubling oscillations. $\eta=0.44$. $V=0.6\ \mu\mathrm{m\ s^{-1}}$. $\lambda=27.4\ \mu\mathrm{m}$ ($\Lambda\approx1.5$). $t=81$ s. The front is out of the figure. The image has been contracted by a factor of 0.5 along the growth direction in order to increase the visibility of the oscillations.

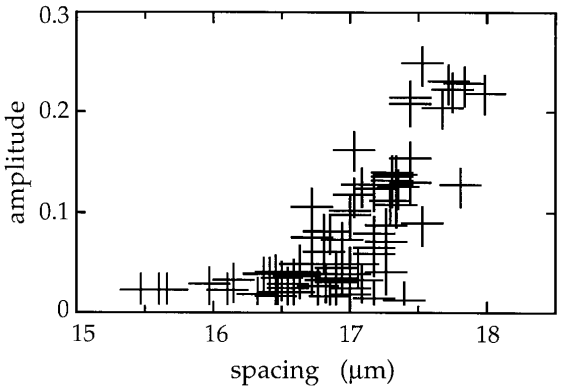

FIG. 22. Reduced oscillation amplitude (dimensionless vs spacing in a sample close to the 2λO bifurcation threshold. $\eta=0.55$. $V=0.82\ \mu\mathrm{m\ s^{-1}}$ ($\lambda_{\mathrm{JH}}\approx16\ \mu\mathrm{m}$).

waves. We only observed this type of response at very low velocity. We measured λ and the oscillation amplitude $A_{2\lambda\mathrm{O}}$, defined as the ratio of the maximum displacement of the junction points to λ, at each point of a broad area, in which several intermittent 2λO patches coexisted with non-oscillating regions. Figure 22 shows the amplitude-spacing correlation diagram obtained in this way. It can be seen that, although $A_{2\lambda\mathrm{O}}$ exhibits a clear tendency toward increasing as λ increases, the local value of $A_{2\lambda\mathrm{O}}$ is not strictly determined by the local value of λ. This fact should be confronted with the following theoretical results: the 2λO bifurcation is subcritical (see Sec. IV B); and localized oscillation pulses can exist within the metastability domain of subcritical Hopf bifurcations, as shown by Fauve and Thual [43]. This suggests that the interval of spacing covered by the oscillation patches more or less coincides with the metastability domain of the bifurcation. According to this assumption, in Fig. 22 the metastability domain would be centered at 16.8 μm ($\Lambda\approx1.22$), and have a width of 0.6 μm ($\delta\Lambda\approx0.04$), in good agreement with the values found numerically by Karma and Sarkissian. On the other hand, independently of this interpretation, Fig. 22 clearly shows that the 2λO bifurcation is very steep. The maximum possible value of $A_{2\lambda\mathrm{O}}$ is $(1-\eta)/2$(≈0.25, in the case considered) since a larger amplitude would mean the termination of the β lamellae. This value is reached for λ only about 1 μm above the threshold ($\delta\Lambda\approx0.07$), which is again in agreement with the numerical

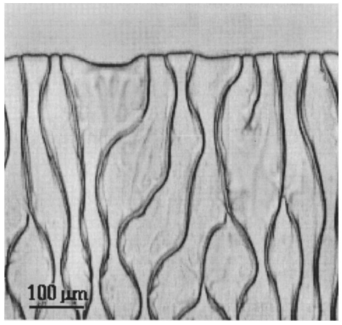

FIG. 23. Interplay between period-doubling oscillation, lamella termination, and lamella branching in a hypoeutectic sample. $\eta=0.12$. $V=0.77\ \mu\mathrm{m\ s^{-1}}$ ($\lambda_{\mathrm{JH}}\approx25\ \mu\mathrm{m}$).

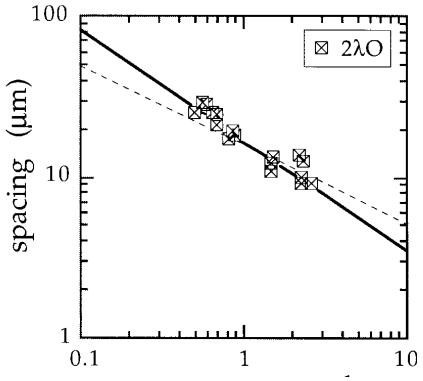

FIG. 24. Spacing vs pulling velocity in the 2λO patterns. Data obtained in the range $0.4 \leqslant \eta \leqslant 0.55$. Continuous line: best-fit power law (exponent -0.7). Broken line: slope -0.5.

results. At larger values of λ, or in response to a further slight increase of V, 2λ oscillations generally do not trigger lamella-termination events, at least in hypereutectic samples. Instead of this, the amplitude of the oscillations saturates slightly below the maximum possible value [see Fig. 10(a)]. In the hypoeutectic range, lamella-termination events do occur when the oscillating amplitude increases, as observed numerically. Note that it is the lamellae of the excess phase (α) that are eliminated. As a result, extremely large α lamellae are formed, which in turn are subject to the lamella-branching instability (see Sec. III D). A disordered regime of interplay between 2λ oscillation, lamella termination, and lamella branching follows (Fig. 23), which generally ends with the emission of solitary tilt waves.

Owing to the small width of the 2λO stability range, it is permissible to assimilate any value of λ measured in the 2λO state to the threshold value $\lambda_{2\lambda O}$. Figure 24 shows a λ-V logarithmic plot of a number of values of λ measured in 2λO states within the concentration range $0.4 < \eta < 0.55$. The exponent of the best-fit power law is 0.7 ± 0.1. This is significantly larger than 0.5. So, as announced above, we find that the 2λO threshold decreases more rapidly than $V^{-1/2}$ as V increases. Since the lamella-termination threshold closely follows the law $\lambda \propto V^{-1/2}$, the width of the basic state stability range at given concentration decreases as V increases. A λ-V logarithmic plot of the time period $t_{2\lambda O}$ of the oscillations is displayed in Fig. 25. The exponent of the best-fit power law is -1.1 ± 0.2. The data points appearing in this figure are averages with respect to the spatial variations of $t_{2\lambda O}$ mentioned in Sec. IV A. In an attempt to explain these variations, we performed local t-λ plots similar to the local A-λ plot shown in Fig. 22. No significant correlation between the local values of $t_{2\lambda O}$ and λ appeared in these diagrams.

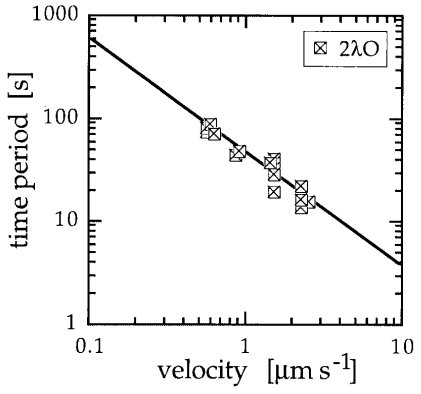

FIG. 25. Time period of the oscillations vs pulling velocity in the 2λO patterns. Same concentration range as in Fig. 24.

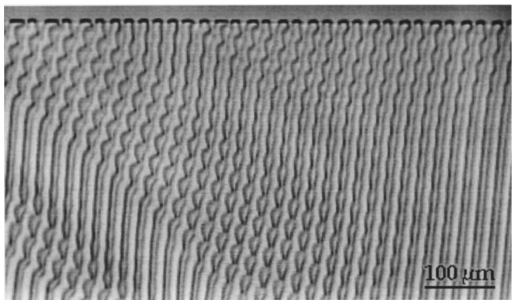

FIG. 26. Response to a V jump from 0.26 to 1 $\mu m\,s^{-1}$. $\eta = 0.44$. The spacing ranges from 22 to 24.3 μm, and the tilt angle from 6.4° to 16.6° depending on the domain considered ($\lambda_{JH} = 13.6$ μm).

We should not close this section without mentioning a previous observation, which is apparently at variance with our present results. This observation is that, in hypoeutectic samples, the basic state is sometimes observed to remain stable up to values of Λ largely above the 2λO threshold. A typical example was given in Fig. 7 of Ref. [18]. In that example, Λ varies from about 1 to 5 over only 20 periods. No oscillations are seen at the crossing of the 2λO threshold (in this case, $\Lambda_{2\lambda O} \approx 1.4$). We are inclined to think that the observed inhibition of the 2λO mode is a nonlinear effect connected with the unusually large gradient of λ. The origin of this gradient is, however, also unclear. It is perhaps induced by some underlying crystallographic defects (subgrain boundaries). However, this has to be confirmed by further studies.

B. Transitions to the tilted states

Kassner and Misbah [25] found numerically that a pure tilt bifurcation exists in our system, but did not study the stability of the basic and tilted states. Fauve, Douady, and Thual [44] showed phenomenologically that, in 1D systems presenting a tilt bifurcation, the tilted state is unstable to long-wavelength perturbations immediately above the tilt bifurcation threshold. Karma and Sarkissian found numerically that, in our system, the basic states and the T states are both unstable in the vicinity of the T-bifurcation threshold, and that, in the hypereutectic range, the stable state of the system in this region is the T-2λO state. Our experimental observations are in agreement with these results. It was previously shown that, for $\eta \approx 0.5$, a homogeneous T state can be obtained from a basic state of spacing close to λ_{JH} by means of V jumps, bringing the system well into the stability domain of the T state [16]. The amplitude of the V jump had to be larger than about 4.5. The response of the system to a V jump of amplitude about 4, bringing the system near the T-bifurcation threshold, is shown in Fig. 26. It can be seen that the frozen-in λ modulation of the sample has been am-

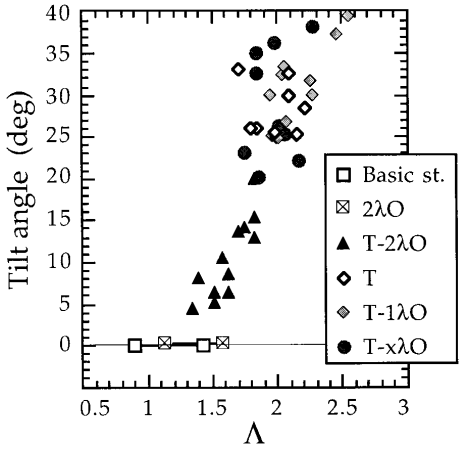

FIG. 27. Tilt angle vs reduced spacing (dimensionless) for all the patterns observed in the range $0.4 \leqslant \eta \leqslant 0.47$.

plified, leading to a pattern in domains, which are all in a T-2λO state, but at different spacings, tilt angles, and oscillation amplitudes. The domains that are formed are homogeneous, and some of them have a very large width ($>20\lambda_m$), leaving no doubt on the stability of their internal state. The formation of domains is thus due to the instability of the basic and T states with respect to long-wavelength λ modulations, the T-2λO state being stable. V jumps of smaller amplitude (typically 3) also lead to patterns in domains (see Fig. 9 of Ref. [16]). The formation of tilt domains is thus the final outcome of the long-wavelength instability predicted in Ref. [44].

The evolution of the tilt angle as a function of Λ through the sequence $2\lambda O \rightarrow T\text{-}2\lambda O \rightarrow T \rightarrow T\text{-}1\lambda O$ in the narrow concentration range $0.42 < \eta < 0.47$ is shown in Fig. 27. It can be seen that, T-xλO points apart, the experimental points form a continuous curve evoking a direct tilt bifurcation, the T-2λO points filling the previously-noticed gap between the 2λO and the T points. As for the T-xλO points, they are clearly off this scheme, occupying the whole range of Λ above the T-2λO domain. We looked for a possible correlation between x and various quantities, such as the spacing, tilt angle, width of the domain, and drift velocity of the domain walls, but did not find any.

In the hypoeutectic range, there is no stability domain for the extended tilted state. The tilt mode nevertheless manifests itself experimentally, particularly in the form of solitary tilt waves. An example is given in Fig. 28. That solitary tilt

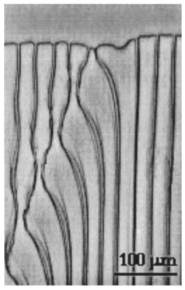

FIG. 28. Solitary tilt wave in a hypoeutectic sample. Same run as in Fig. 10(b).

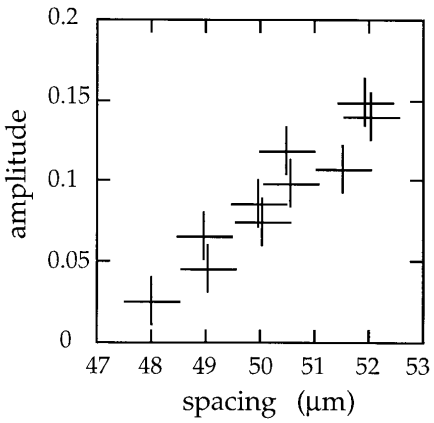

FIG. 29. Reduced oscillation amplitude (dimensionless) vs spacing in the 1λO pattern. Same run as in Fig. 13. $\lambda_{JH} \approx 20.0$ μm.

waves are clearly distinct from tilt domains seems not to have been stressed before this. Tilt domains are of an arbitrarily large width, and their internal state is homogeneous, and independent of their width (see Fig. 8). Their existence relies on that of a stability domain of the T state. In contrast, solitary tilt waves have a definite, small width (typically, 2λ or 3λ), and no well-defined internal state. They can exist even if there exists no stability domain of the tilted states. Solitary tilt waves are also encountered in the hypereutectic range. In this range, however, they are fragile, and generally

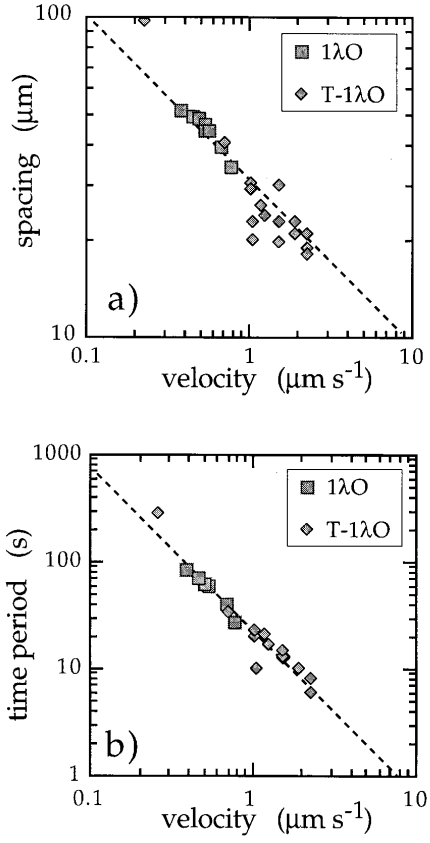

FIG. 30. Period-preserving oscillatory patterns. (a) Spacing vs pulling velocity; broken line: slope −0.5. (b) Oscillation time period vs pulling velocity; broken line: slope −1.5.

end by transforming into tilt domains. Another experimentally observed characteristic of solitary tilt waves is that they are leaving behind a wake of decaying 2λ oscillations.

C. 1λO primary bifurcation and the transition $T \rightarrow T$-1λO

Figure 29 shows an amplitude-spacing correlation diagram obtained in a 1λO state. It can be seen that, within experimental uncertainty, the local value of the oscillation amplitude is entirely determined by the local value of the spacing. Figure 29 is thus the bifurcation diagram of the 1λO bifurcation. The steepness of the bifurcation curve is comparable with the one obtained numerically by Karma and Sarkissian, but the metastability domain found by these authors is not detected experimentally. The dependence of the local state on the local value of λ extends to higher values of λ, well into the 1λ-2λO domain (results not shown).

As in the case of the 2λO bifurcation, the narrowness of the 1λO domain allows us to assimilate any value of λ measured in a 1λO state to the threshold value $\lambda_{1\lambda O}$. An experimentally-measured $\lambda_{1\lambda O}$ vs V logarithmic plot is shown in Fig. 30(a). This plot is compatible with $\lambda_{1\lambda O}$ following the law $\lambda \propto V^{-1/2}$. A logarithmic plot of the oscillation time period $t_{1\lambda O}$ as a function of V is given in Fig. 30(b). The data suggest a law $t_{1\lambda O} \propto V^{-3/2}$. This implies that the wavy solidification microstructures left behind in the solid at different velocities are geometrically similar to each other ($\lambda \propto tV \propto V^{-1/2}$).

The data corresponding to T-1λO states are also displayed in Fig. 30. Naturally, since the domain of existence of the T-1λO states is large, the error made in assimilating the measured values of λ with the threshold values is large. Nevertheless, it can be seen that the points corresponding to the T-1λO states roughly fall on the same straight lines as those corresponding to the 1λO states, suggesting that the 1λ oscillations are practically insensitive to whether the pattern is tilted or not. On the other hand, we did not succeed in stabilizing small-amplitude T-1λO states. Small-amplitude T-1λ oscillation were invariably observed to die out with time. The only permanent homogeneous T-1λO states that we observed had large oscillation amplitude, comparable to the one shown Fig. 9. Probably, the $T \rightarrow T$-1λO bifurcation is subcritical, with a much larger metastability domain than the primary 1λO bifurcation. However, this point remains to be clarified.

VI. CONCLUSION

Some conclusions of general interest can be drawn from this study. We are now in a position to discuss the old wavelength-selection conjecture. The question is the following [46]: Do directionally solidified lamellar eutectics pulled at constant velocity basically tend toward a unique ''selected'' state independent of the history of the sample? Secondarily, does the selected state, if any, correspond to the smallest possible average undercooling of the front? The results reported above clearly are in favor of a negative answer to the first of these questions, rendering the second one irrelevant. The stability diagram established for our system indicates that the system can permanently assume a variety of homogeneous or nonhomogeneous states depending on the history of the sample. We have given much direct experimental evidence of this multistability. The range of interlamellar spacing covered by these various possible states (the operating range of the system) is relatively large in very thin samples (the ratio of its upper bound to its lower bound being larger than two). It is probably smaller, but still finite, in bulk samples. The bounds of the operating range, and the instability thresholds of the various states are decreasing functions of V, but do not strictly follow a $V^{-1/2}$ law. We believe that these conclusions are not specific of the particular system studied here, but generic for lamellar eutectics.

The preceding conclusion can be formulated in a different way: we have found no mechanism of selection capable of bringing the system from an arbitrary initial state to a unique, selected state. A mechanism based on phase diffusion was once proposed by Langer [47], but neither phase diffusion, nor, consequently, Langer's marginal-stability mechanism, are observed to occur in lamellar eutectics, at least on a realistic time scale. On the other hand, a genuine mechanism of wavelength selection can actually operate in lamellar eutectics, namely, the so-called dynamical wavelength selection by tilt domains, but dynamical wavelength selection by tilt domains takes place under such restrictive conditions that it can by no means ensure wavelength selection in general. Moreover, this mechanism provides a counterexample to the principle of minimum undercooling since it leads (when it takes place) to the selection of a wavelength λ^* bearing no relation with the minimum-undercooling wavelength λ_m, as shown, in particular, by the fact is that λ^* and λ_m do not vary with V in the same way [17].

More positively, this work establishes that the minimal model used in the numerical calculations is a true picture of lamellar eutectic growth, justifying our assumption that anisotropy effects are weak in the so-called floating eutectic grains. That this conclusion can be applied to all lamellar eutectics, in particular, to metallic ones, remains to be directly proven, but seems very probable. Many of the morphological instabilities that we have observed in CBr_4-C_2Cl_6 have also been encountered in directionally solidified [48] and laser-solidified [38,45] metallic eutectics, and metallic-salt eutectics [10]. Our study also proves that 3D effects are weak in samples of thickness comparable to the wavelength of the patterns. Therefore, provided that the appropriate precautions—in particular, those concerning the size and the nature of the eutectic grains, and the thickness of the samples—are taken, directional solidification of thin samples of binary lamellar eutectics seems to be one of the most promising types of experimental systems for the study of the fine details of the nonlinear dynamics of modulated fronts.

Concerning possible metallurgical applications, a major question left open by our work is whether or not the results obtained for a 2D system are relevant to bulk samples. Modifications due to the convection flows in the liquid apart, the basic state of lamellar eutectics is the same in bulk as in thin samples. The difference between the two cases is that the 3D instabilities are active in bulk samples while they are largely blocked in thin samples. Therefore, the question is to identify the 3D instabilities of the basic state, and to determine the location of their thresholds in the parameter space. If these thresholds fall well inside the 2D stability domain of the

basic state, the stability diagram established above will probably be of little use for bulk samples. It seems that very little is known about the 3D instabilities of bulk lamellar eutectics. Much attention has been paid in the past to the linear faults appearing on the transverse cross sections of bulk samples of metallic lamellar eutectics, but the origin, the behavior, and the part actually played by these defects in the growth dynamics, are still obscure [45]. In future, 3D instabilities should be one of the central topics of the research on lamellar eutectic growth.

ACKNOWLEDGMENTS

We thank A. Karma and A. Sarkissian for communicating their results prior to publication. We also gratefully acknowledge many stimulating discussions with C. Caroli and A. Karma. Thanks are also due to H. Savary and A.-M. Pougnet, of the Centre National d'Etudes des Télécommunications, France-Telecom, Bagneux, France, for providing us with zone-refined chemicals. This research was financially supported by the Centre National d'Etudes Spatiales, France.

[1] J. D. Hunt and K. A. Jackson, Trans. AIME **236**, 843 (1966).

[2] The morphological instabilities of the lamellar eutectic growth fronts present profound similarities with those of other one-dimensional periodically modulated fronts. The general, phenomenological reasons for this fact are now well known [M. R. E. Proctor and C. A. Jones, J. Fluid Mech. **188**, 301 (1988); P. Coullet and G. Iooss, Phys. Rev. Lett. **64**, 866 (1990)]. The experimental illustrations of it are too numerous to be quoted here. We refer the interested reader to P. Oswald, J. Bechhoefer, and A. Libchaber [*ibid.* **58**, 2318 (1987)] and J.-M. Flesselles, A. J. Simon, and A. Libchaber [Adv. Phys. **40**, 1 (1991)] as concerns directionally solidified liquid crystals; to M. Rabaud, S. Michalland, and Y. Couder [Phys. Rev. Lett. **64**, 184 (1990)] as concerns directional viscous fingering; and to F. Giorgiutti, A. Bleton, L. Limat, and J. E. Weisfried [*ibid.* **74**, 538 (1995)] as concerns the dynamics of one-dimensional arrays of liquid columns. In all these systems save the last one, the basic state is planar, and the stationary periodic state, i.e., the state having the same symmetries as the basic state of lamellar eutectics, results from a primary bifurcation from the planar state, as shown a long time ago by W. W. Mullins and R. F. Sekerka [J. Appl. Phys. **35**, 444 (1964)] in the case of directionally solidified dilute alloys. For this reason, the bifurcations called ''primary'' in this paper are considered ''secondary'' by the authors studying the above-mentioned systems.

[3] A. Karma and A. Sarkissian, Metall. Mater. Trans. A **27**, 635 (1996).

[4] G. A. Chadwick, Prog. Mater. Sci. **12**, 97 (1963).

[5] The deviations from what would be a perfect selection of the growth pattern in directionally solidified lamellar eutectics were seriously taken into consideration relatively recently G. Lesoult [Ann. Chim. (France) **5**, 154 (1980)] carried out a detailed compilation of the measured average values of λ as a function of V in metallic eutectics, and found that the deviations from the law $\lambda \propto V^{-1/2}$ are often large. R. Trivedi, J. T. Mason, J. D. Verhoeven, and W. Kurz [Metall. Trans. A **22**, 2523 (1991)] determined the histogram of the local values of λ in a number of lead-based eutectic alloys, and found that the width of this histogram is typically of 20% of the average value, and often more.

[6] K. A. Jackson and J. D. Hunt, Trans. AIME **236**, 1129 (1966).

[7] B. Caroli, C. Caroli, and B. Roulet, in *Solids Far from Equilibrium*, edited by C. Godrèche (Cambridge University Press, Cambridge, 1992). In directional solidification, the term (one-sided) minimal model designates a theory in which the hydrodynamics flows in the liquid, the rejection of latent heat by the solid, the mass diffusion in the solid, the attachment kinetics at the interface, and the orientation dependence of the surface tension (capillary anisotropy) are neglected. The equations of the model are the diffusion equation for the solute concentration in the liquid ahead of the front, the mass conservation equation for the solute, and the Gibbs-Thomson equation at the solid-liquid interfaces. In the case of eutectics, one adds the Young equation at the α-β-liquid junction lines (or points, in 2D systems).

[8] W. Datye and J. S. Langer, Phys. Rev. B **24**, 4155 (1981).

[9] A. Karma, Phys. Rev. Lett. **59**, 71 (1987).

[10] The $2\lambda O$ and T modes were experimentally discovered, and studied in some detail by J. Van Suchtelen in thin samples of the transparent eutectics $PbCl_2$-CuCl and NaCl-CuCl during the 1970s [J. Van Suchtelen, (unpublished)]. The T mode had been previously occasionally observed in CBr_4-C_2Cl_6 by K. A. Jackson in 1967 [quoted by J. S. Kirkaldy, Rep. Prog. Phys. **55**, 723 (1992), Fig. 46].

[11] W. L. Kaukler and J. W. Rutter, Mater. Sci. Eng. **65**, L1 (1984).

[12] V. Seetharaman and R. Trivedi, Metall. Trans. A **19**, 2955 (1988).

[13] G. Faivre, S. de Cheveigné, C. Guthmann, and P. Kurowski, Europhys. Lett. **9**, 779 (1989).

[14] J. Mergy, thèse de doctorat de l'Université Paris-7, 1992.

[15] B. Caroli, C. Caroli, G. Faivre, and J. Mergy, J. Cryst. Growth **118**, 135 (1992).

[16] G. Faivre and J. Mergy, Phys. Rev. A **45**, 7320 (1992).

[17] G. Faivre and J. Mergy, Phys. Rev. A **46**, 963 (1992).

[18] J. Mergy, G. Faivre, and R. Mellet, J. Cryst. Growth **13**, 353 (1993).

[19] G. Faivre, J. Cryst. Growth **166**, 23 (1996).

[20] K. Brattkus, B. Caroli, C. Caroli, and B. Roulet, J. Phys. (France) **51**, 1847 (1990).

[21] B. Caroli, C. Caroli, and B. Roulet, J. Phys. (France) **51**, 1865 (1990).

[22] B. Caroli, C. Caroli, and S. Fauve, J. Phys. (France) I **2**, 281 (1992).

[23] K. Kassner and C. Misbah, Phys. Rev. Lett. **66**, 445 (1991); J. Phys. A **25**, 3213 (1992).

[24] K. Kassner and C. Misbah, Phys. Rev. A **44**, 6513 (1991).

[25] K. Kassner and C. Misbah, Phys. Rev. A **44**, 6533 (1991); A. Valance, C. Misbah, D. Temkin, and K. Kassner, Phys. Rev. E **48**, 1924 (1993).

[26] K. Kassner and C. Misbah, Phys. Rev. A **45**, 7372 (1992).

[27] K. Kassner, A. Valance, C. Misbah, and D. Temkin, Phys. Rev. E **48**, 1091 (1993).
[28] R. Bauman, K. Kassner, C. Misbah, and D. E. Temkin, Phys. Rev. Lett. **74**, 1597 (1995).
[29] W. Kurz and D. J. Fischer, in *Fundamentals of Solidification* (Trans Tech Aedermannsdorf, 1984), p. 109. The transition from the ''planar'' regimes to the regimes of dendrites and ''colonies'' takes place above a critical value of the ratio V/G, which is a function of C and the residual-impurity content [F. R. Mollard and M. C. Flemings, Trans. AIME **239**, 1534 (1967)]. The planar coupled zone is the zone of the parameter space situated below this critical value of V/G.
[30] S. Akamatsu, G. Faivre, and T. Ihle, Phys. Rev. E **51**, 4751 (1995).
[31] S. Akamatsu and G. Faivre, J. Phys. (France) I **6**, 503 (1996).
[32] F. R. Mollard and M. C. Flemings, Trans. AIME **239**, 1526 (1967).
[33] L. M. Hogan, R. W. Kraft, and F. D. Lemkey, Adv. Mater. Res. **5**, 83 (1971).
[34] W. A. Tiller K. A. Jackson, J. W. Rutter, and B. Chalmers, Acta Metall. **1**, 498 (1953).
[35] By orientation of a eutectic grain, we mean the set of six angular variables, three of which specify the orientation of the crystal lattice of, say, the α phase with respect to the laboratory reference frame, the three others specifying the orientation of β with respect to α. Similarly, the capillary anisotropy within a given eutectic grain is described by the three functions (Wulff plots) giving the dependence of the α-liquid, β-liquid, and α-β interfaces on the orientation of their normal with respect to, say, the laboratory reference frame. The α-liquid and β-liquid Wulff plots of two different grains are simply rotated with respect to each other, but, in general, the α-β Wulff plots are entirely different. The (rare) grains, the α-β Wulff plot of which have cusps are called locked grains because, in such grains, the eutectic lamellae are generally locked onto the orientation(s) corresponding to the cusp(s) of the α-β Wulff plot [15]. The grains, the α-β Wulff plot of which presents no singularity are called ''floating grains.''
[36] Dynamical wavelength selection by tilt domains was first experimentally observed in a nematic-isotropic front by A. J. Simon, J. Bechhoefer, and A. Libchaber [Phys. Rev. Lett. **61**, 2574 (1988)]. A phenomenological theory of its was proposed by P. Coullet, R. E. Goldstein, and G. H. Gunaratne [*ibid.* **63**, 1954 (1989)] and Caroli *et al.* [22]. It was experimentally studied in detail in thin samples of CBr_4-C_2Cl_6 by Faivre and Mergy [17], who found that the dynamically-selected spacing λ^* roughly decreases as V^{-1} as V increases.
[37] There exists a profusion of denominations for the various modes of instability of 1D modulated fronts. The tilt mode is also called the symmetry-breaking, parity-breaking, propagating, or traveling mode. The $2\lambda O$ mode is called vacillation breathing by K. Kassner, C. Misbah, and H. Müller-Krumbhaar [Phys. Rev. Lett. **67**, 1551 (1991)]. The $1\lambda O$ mode is sometimes called optical mode, and the $x\lambda O$ modes of arbitrary x, irrational modes.
[38] M. Zimmermann, A. Karma, and M. Carrard, Phys. Rev. B **42**, 833 (1990).
[39] G. Faivre, C. Guthmann, and J. Mergy, in *Nonlinear Phenomena in Materials Science*, edited by L. Kubin and G. Martin (Trans Tech, Aedermannsdorff, 1992), Vol. 2, p. 1.
[40] R. N. Grugel, T. A. Lograsso, and A. Hellawell, Metall. Trans. A **15**, 1003 (1984).
[41] S. C. Gill and W. Kurz, Acta Metall. Mater. **41**, 3563 (1993).
[42] M. Ginibre (unpublished).
[43] S. Fauve and O. Thual, Phys. Rev. Lett. **64**, 282 (1990).
[44] S. Fauve, S. Douady, and O. Thual, Phys. Rev. Lett. **65**, 385 (1990); J. Phys. (France) II **1**, 311 (1991).
[45] H. Dean and J. E. Gruzleski, J. Cryst. Growth **21**, 51 (1974).
[46] C. Caroli and G. Faivre, in *Nonlinear Phenomena in Materials Science*, edited by G. Anandakrishna (Trans Tech, Aedermannsdorff, 1996), Vol. III.
[47] J. S. Langer, Phys. Rev. Lett. **44**, 1023 (1980).
[48] H. E. Cline, Metall. Trans. A **15**, 1013 (1984); Mater. Sci. Eng. **65**, 93 (1984).